Modelling Bifacial Solar Energy Yield for Single-Axis Tracked Systems with Racking

Annie C. J. Russell[1], Christopher E. Valdivia[1], Mandy R. Lewis[1], Joan E. Haysom[1,2], Karin Hinzer[1]
[1]SUNLAB, Centre for Research in Photonics, University of Ottawa, Ottawa, ON, Canada
[2]J.L. Richards & Associates Limited, Ottawa, ON, Canada

***Abstract*—This paper presents a bifacial PV energy yield simulation tool with highly-parameterized optical and electrical models. The resulting detailed irradiance profiles provide insight into the effects of rack shading. Horizontal parallel wiring architecture of cells in the module is found to mitigate non-uniform rear irradiance caused by torque tube shading in a single-axis tracked system for representative cloudy and clear days. Low cell shunt resistance is shown to amplify bifacial gain during low irradiance hours. Annual energy yield predictions for fixed and tracked bifacial PV systems for Ottawa, ON are also presented.**

***Keywords*—Photovoltaics, bifacial, solar irradiance, single-axis tracking, energy yield, bifacial gain, shunt resistance, panel wiring**

I. Introduction

Bifacial photovoltaic (PV) modules, which collect light from both front and rear sides, are expected to make up 35% of the world crystalline silicon market share by 2027 [1]. However, the numerous factors affecting bifacial PV energy generation have yet to be fully quantified, and this uncertainty forms a major barrier to investment [2]. The proposed bifacial PV energy yield model contains highly-parameterized optical and electrical models and provides insight into the factors affecting bifacial yield on hourly to annual time scales, including environmental conditions, rack shading, shunt resistances, and non-uniform rear irradiance.

II. Model Description

The simulation considers an array of solar panels situated at the center of a flat surface under a sky dome. Irradiance profiles and hourly power output are calculated for a specified solar module under investigation (MUI).

A. Array Geometry

An adjustable number of rows, tiers, and panels are arranged in a fixed-tilt or single-axis tracked array. For a *1-up* (single tier) single-axis tracker (Fig. 1b), panels rotate around a horizontal, north-south oriented torque tube at an optimal hourly tilt [3]. Rack posts and the torque tube are modeled as cylinders, defined by a radius and a central line between two end points.

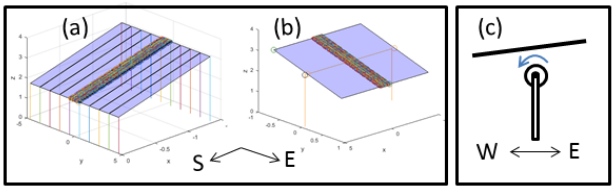

Fig. 1: Geometry for (a) fixed-tilt system and (b) single-axis tracking system with cross-section as in (c). Not to scale.

B. Optical Models

The model maps direct sunlight, diffuse anisotropic sky radiation, and ground-reflected light to the MUI. The sky dome, isotropically-reflective ground surface, and MUI are partitioned into patches that are coupled by light rays.

Eq. (1)-(2), for which variables are described in Table 1, express $P_{o,m}$ - the optical power incident on a front or rear side module patch due to light originating from the sun, sky, or ground,

$$P_{o,m} = G_{o,m} \cdot IAM(\theta_{o,m}) \cdot T \cdot A_c \quad (1)$$

$$G_{o,m} = G_o \cdot \cos(\theta_{o,m}) \cdot \delta_{o,m} \quad (2)$$

where the source irradiance $G_o = G_s$ is the sky-patch irradiance via Perez model [4] in the diffuse light case, or the direct normal irradiance for the direct sunlight case. For ground-reflected light from both diffuse and direct sources, $G_o = G_g$ as in (3), where G_s is as defined above,

$$G_g = G_s \cdot \cos(\theta_{s,g}) \cdot \Omega_{g,m} \cdot \delta_{s,g} \cdot \rho \cdot \alpha \quad (3)$$

The hourly albedo, ρ, governs the Lambertian reflection. $\delta_{o,m}$ and $\delta_{s,g}$ are shading factors applied to the rays between coupled patches. If the minimum distance between a ray and a rack central line is found to be less than the rack radius, the ray is blocked and the shading factor is set to zero. δ is set to a transparency factor if the ray intersects with a row of panels.

TABLE I. Optical Model Variable Definitions

Variable	Description
$G_{o,m}$	Incident irradiance at module patch (m) due to optical source (o, i.e. sky or ground patch, or sun)
G_o, G_s & G_g	Origin light source irradiance; o=s for sky patches and direct sunlight, and o=g for ground-reflected light
$\theta_{o,m}$ & $\theta_{s,g}$	Angle of incidence between origin light source and module (o,m) or sky/sun source and ground patch (s,g)
$\delta_{o,m}$ & $\delta_{s,g}$	Shading factor between optical source and module (o,m) or sky/sun source and ground patch (s,g)
ρ	Albedo (reflectivity of the ground cover)
$\Omega_{g,m}$	Solid angle between ground patch and module patch
α	Compensation factor to account for computational errors resulting from finite ground patching area
$IAM(\theta_{o,m})$	Incidence angle modifier
T	Module transmittance through encapsulation layers on the incident face (front or rear)
A_c	Area of cell in the module patch.

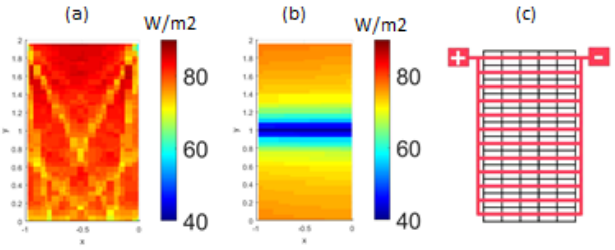

Fig. 2: Rear irradiance profiles for a cloudy January hour at noon with (a) fixed-tilt with vertical racking and (b) single-axis tracking with torque tube (5 cm radius). (c) Parallel wiring architecture in a panel with 12 parallel strings.

The sum of the module patch irradiances due to each optical source forms a detailed front and rear irradiance profile (rear profiles shown in Fig. 2 a,b).

C. Photovoltaic Model

The optical power of all front and rear module patches is mapped to each cell as P_f and P_r. Eq. (4) gives the photo-generated short circuit current of each cell (I_{sc}) where φ is the rear current de-rate, or *bifaciality factor* (set to 0.95), and R is the responsivity in A/W.

$$I_{sc} = \left(P_f + P_r \cdot \varphi\right) \cdot R \qquad (4)$$

Cell current-voltage (*I-V*) behaviour is governed by a temperature-dependent single diode model with adjustable cell parameters including shunt resistance. Cell parameters are regressed from an experimental *I-V* curve.

The 72 cell *I-V* curves are summed, as dictated by the specified wiring architecture, to form the total panel *I-V* behaviour. Inter-cell wiring can range from a single (series) string to 12 parallel strings, as in Fig. 2c. The MUI maximum power point is found for each hourly time step.

III. Results & Discussion

Hourly and annual energy yield calculations were performed for a MUI at the center of a single row of 9 panels in portrait orientation for both a fixed latitude-tilt and a 1-up north-south single-axis tracked configuration. The geographic and historical meteorological conditions were set for Ottawa, Canada.

For the 1-up tracked configuration with 4-9 cm torque tube radii, daily loss in bifacial yield due to rack shading ranges from 3-9% and 1-4% for representative cloudy and clear January days respectively. For a 4-6 cm torque tube radius, 5% of this cloudy day shading loss can be mitigated by increasing the distance between the torque tube and the panels to 25 cm. In addition, Fig. 3 shows that parallel wiring increases yield as compared to the series configuration (referred to as *parallel gain*), with the effects of non-uniform rear irradiance best mitigated when every row of cells constitutes a separate parallel string. Three strings give a higher yield than two and four as the torque tube shading limits only the central string current.

The bifacial tracked system demonstrates an annual *tracking gain* of 14.0% as compared to the bifacial fixed-tilt system. The monofacial tracking gain is higher (16.6%) since bifacial fixed-tilt systems already harvest a significant portion of the rear-incident light that is available in the tracked system. Fig. 4 shows a loss in both bifacial and monofacial tracking yield vs. fixed yield during winter months, due to low sun elevation angles; this effect could be mitigated by double-axis tracking.

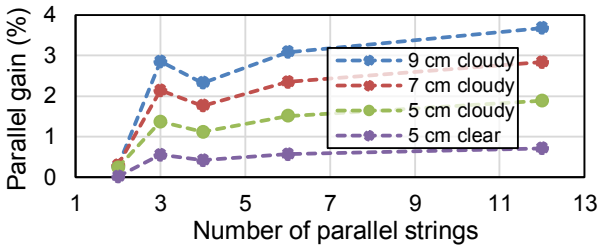

Fig. 3: Parallel gain for multiple torque tube radii (5-9 cm)

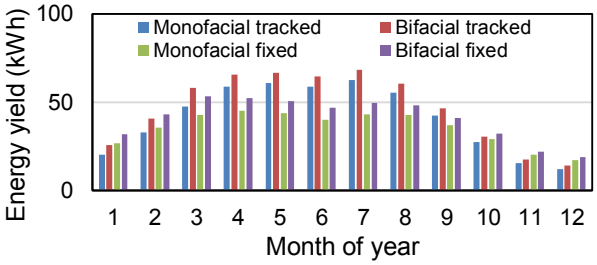

Fig. 4: Monthly bifacial and monofacial energy yield for fixed-tilt and single-axis tracked systems.

Both rack shading and environmental factors, such as ground albedo, strongly affect the *bifacial gain* (i.e. increase in yield of bifacial over monofacial modules). Additionally, Fig. 5 shows that low shunt resistances dampen monofacial power to a greater extent than bifacial power during low irradiance periods (due to lower monofacial I_{sc}), leading to higher apparent gains. This effect is most prominent under high proportions of diffuse light.

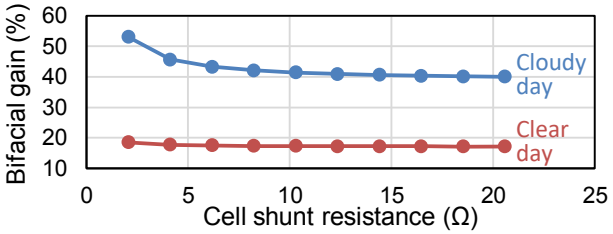

Fig. 5: Effect of shunt resistance on bifacial gain.

Full parameterization of the module-level electrical model and system-level optical models allows for a thorough examination of the factors affecting bifacial PV energy yield. This will facilitate future bifacial PV system optimization and increase investor confidence for earlier deployments in this expanding market segment.

[1] VDMA German Engineering Federation, "International Technology Roadmap for Photovoltaics – Results 2017, Ninth Ed.", 2018

[2] J. Libal, "Impact of bifaciality on the levelized cost of PV-generated electricity" in Bifacial Photovoltaics: Technology, applications and economics, R. Kopecek; J. Libal, London, UK: IET, 2018, pp.221-236

[3] W. F. Marion & A. P. Dobos, "Rotation Angle for the Optimum Tracking of One-Axis Trackers," NREL/TP-6A20-58891, July 2013.

[4] R. Perez, R. Seals, & J. Michalsky, "All-weather model for sky luminance distribution-Preliminary configuration and validation," Sol. Energy, vol. 50, no. 3, pp. 235–245, 1993.